Inorg. Chem. **2006**, *45*, 8990–8997

Functionalities of One-Dimensional Dynamic Ultramicropores in Nickel(II) Coordination Polymers

Shin-ichiro Noro,*,† Ryo Kitaura,‡ Susumu Kitagawa,*,‡ Tomoyuki Akutagawa,† and Takayoshi Nakamura†

Research Institute for Electronic Science, Hokkaido University, Sapporo 060-0812, Japan, and Department of Synthetic Chemistry and Biological Chemistry, Graduate School of Engineering, Kyoto University, Katsura, Nishikyo-ku, Kyoto 615-8510, Japan

Received June 12, 2006

Ni^{II} coordination polymers with a 4,4′-azobis(pyridine) (azpy) ligand, $\{[Ni_2(NCX)_4(azpy)_4]\cdot G\}_n$ (X = S, G (guest molecule) = MeOH (**1**·MeOH); X = S, G = EtOH (**1**·EtOH); X = S, G = H_2O (**1**·H_2O); X = S, G = no guest (**1**); X = Se, G = MeOH (**2**·MeOH); X = Se, G = H_2O (**2**·H_2O); X = Se, G = no guest (**2**)), have been synthesized and structurally characterized with their porosity. These compounds have one-dimensional periodic ultramicropores that contain the small guest molecules, H_2O, MeOH, or EtOH, whose hydroxy groups interact with the S or Se atoms of isothiocyanate or isoselenocyanate, respectively, via –S(Se)···HO– hydrogen bonds. Although the molecular dimensions of the MeOH guest are considerably larger than the window size of the ultramicropore, **1**·MeOH and **2**·MeOH easily release their guest molecules without decomposition of the framework to form **1** and **2** without any guest molecules. This shows that **1** and **2** have dynamic ultramicropores constructed from the interpenetrating framework. The guest desorption experiments using **1**·MeOH and **1**·EtOH reveal that the difference in the desorption behavior is due to van der Waals interactions that depend on the molecular shape of the guest molecule in the ultramicropores and/or an entrance blocking effect that depends on the minimum dimensions of the guest molecule for the pore windows. A marked difference in the N_2 and CH_4 adsorption isotherms was observed and is associated with the strength of the host–guest interaction.

Introduction

A new class of porous materials, known as coordination polymers, constructed from transition metal ions and organic bridging ligands acting as connectors and linkers, respectively, have attracted a great deal of attention recently, and considerable research effort has been devoted to the development, design, and synthesis of novel porous metal−organic frameworks.[1,2] Porous coordination polymers have advantages over conventional porous materials, such as activated carbons and zeolites: (1) They have well-regulated and designable micropores. (2) They have a variety of micropores ranging from one- to three-dimensional (1-D, 2-D, and 3-D) types. (3) They have a dynamic porous framework constructed by coordination bonds and supramolecular interac-

* To whom correspondence should be addressed. E-mail: noro@es.hokudai.ac.jp (S.N.), kitagawa@sbchem.kyoto-u.ac.jp (S.K.).

† Hokkaido University.

‡ Kyoto University.

(1) (a) Kitagawa, S.; Noro, S. In *Comprehensive Coordination Chemistry II: From Biology to Nanotechnology*; McCleverty, J. A., Meyer, T. J., Eds.; Pergamon Press: Oxford, U.K., 2003; Vol. 7, pp 231−261. (b) Kitagawa, S.; Kitaura, R.; Noro, S. *Angew. Chem., Int. Ed.* **2004**, *43*, 2334−2375. (c) Uemura, K.; Kitagawa, S. *Chem. Soc. Rev.* **2005**, *34*, 109−119. (d) Kitagawa, S.; Noro, S.; Nakamura, T. *Chem. Commun.* **2006**, 701−707.

(2) (a) Oh, M.; Carpenter, G. B.; Sweigart, D. A. *Acc. Chem. Res.* **2004**, *37*, 1−11. (b) Yaghi, O. M.; O'Keeffe, M.; Ockwig, N. W.; Chae, H. K.; Eddaoudi, M.; Kim, J. *Nature (London)* **2003**, *423*, 705−714. (c) Janiak, C. *Dalton Trans.* **2003**, 2781−2804. (d) James, S. L. *Chem. Soc. Rev.* **2003**, *32*, 276−288. (e) Moulton, B.; Zaworotko, M. J. *Curr. Opin. Solid State Mater. Sci.* **2002**, *6*, 117−123. (f) Kim, K. *Chem. Soc. Rev.* **2002**, *31*, 96−107. (g) Evans, O. R.; Lin, W. *Acc. Chem. Res.* **2002**, *35*, 511−522. (h) Moulton, B.; Zaworotko, M. J. *Chem. Rev.* **2001**, *101*, 1629−1658. (i) Kesanli, B.; Lin, W. *Coord. Chem. Rev.* **2003**, *246*, 305−326. (j) Tong, M.-L.; Chen, H.-J.; Chen, X.-M. *Inorg. Chem.* **2000**, *39*, 2235−2238. (k) Férey, G.; Mellot-Draznieks, C.; Serre, C.; Millange, F.; Dutour, J.; Surblé, S.; Margiolaki, I. *Science* **2005**, *309*, 2040−2042. (l) Rosseinsky, M. J. *Microporous Mesoporous Mater.* **2004**, *73*, 15−30. (m) Lee, E. Y.; Jang, S. Y.; Suh, M. P. *J. Am. Chem. Soc.* **2005**, *127*, 6374−6381. (n) Abrahams, B. F.; Moylan, M.; Orchard, S. D.; Robson, R. *Angew. Chem., Int. Ed.* **2003**, *42*, 1848−1851. (o) Mori, W.; Takamizawa, S.; Nozaki-Kato, C.; Ohmura, T.; Sato, T. *Microporous Mesoporous Mater.* **2004**, *73*, 31−46. (p) Ohmori, O.; Kawano, M.; Fujita, M. *Angew. Chem., Int. Ed.* **2005**, *44*, 1962−1964. (q) Ohishi, S.; Ohmori, T.; Ohkubo, T.; Noguchi, H.; Di, L.; Hanzawa, Y.; Kanoh, H.; Kaneko, K. *Appl. Surf. Sci.* **2002**, *196*, 81−88.

10.1021/ic061052d CCC: $33.50
Published on Web 10/06/2006

tions (e.g., hydrogen bonds, $\pi-\pi$ interactions, and CH$-\pi$ interactions), which are weaker than covalent bonds. A large number of researchers have afforded stable, highly porous coordination polymers, which generally have micropores 0.5−2 nm in size for use as novel adsorbents and catalysts. On the other hand, ultramicropores, with a pore size of <0.5 nm, have several characteristic features as follows: (1) The guest molecules are strongly confined in the ultramicropore without any chemical interaction due to a deep, van der Waals-type, potential energy well. (2) An entrance blocking effect is present that depends on the relationship between the pore window size and the molecular dimensions of the guest molecules. (3) Real 0-D or 1-D structures, each of which is well separated, can be formed. Such restricted spaces can be used as a reaction vessel, in which unprecedented physical phenomena are observed.

There have been some reports on the functionalities of ultramicropores formed in coordination polymers.[3−5] For example, $\{[M_2(4,4'\text{-bpy})_3(NO_3)_4]\cdot 2G\}_n$ (4,4′-bpy = 4,4′-bipyridine; M = Co, G = H_2O;[4a] M = Co, G = CS_2;[4b] M = Ni, G = EtOH)[4c,d] has a tongue-and-groove-type structure, which produces channels of cavities with dimensions of 3.6 × 7.6 Å^2 linked by windows with dimensions of 2.3 × 2.8 Å^2 arranged parallel to the crystallographic *a*-axis. The porous Co material has the capacity to adsorb a supercritical gas, such as CH_4, O_2, or N_2, at room temperature and low pressure.[4a] The detailed adsorption dynamics of the porous Ni material have been investigated.[4c,d]

We have also investigated the characteristic porous functionalities of the ultramicroporous coordination polymer $[Cu_2(pzdc)_2(pyz)]_n$ (pzdc = pyrazine-2,3-dicarboxylate and pyz = pyrazine), which has ultramicropores with dimensions of ca. 4 × 6 Å^2 arranged along the crystallographic *a*-axis.[6] Several simple gas molecules can be incorporated into its restricted ultramicropore space in characteristic states, which are not observed in porous materials having micropores or mesopores.[5]

In this paper we report on the synthesis, crystal structure, and porous functionalities of novel coordination polymers with the general formula $\{[Ni_2(NCX)_4(azpy)_4]\cdot G\}_n$ (azpy = 4,4′-azobis(pyridine); X = S, G = MeOH (**1**·MeOH); X = S, G = EtOH (**1**·EtOH); X = S, G = H_2O (**1**·H_2O); X = S, G = no guest (**1**); X = Se, G = MeOH (**2**·MeOH); X = Se, G = H_2O (**2**·H_2O); X = Se, G = no guest (**2**)). These compounds have 1-D dynamic ultramicropores formed by the interpenetrating framework. The details of the crystal structures, host−guest interactions, framework stability and flexibility, substituent effect, and guest adsorption and desorption properties will be discussed below.

Experimental Section

Materials. All the chemicals and solvents used in the syntheses were reagent grade. The 4,4′-azobis(pyridine) ligand was prepared according to a literature method.[7]

Caution! Perchlorate salts are dangerous (especially if they are dry) and should be handled with care.

Synthesis of $\{[Ni_2(NCS)_4(azpy)_4]\cdot MeOH\}_n$ (1·MeOH). The single crystals were obtained using a standard diffusion method in a straight glass tube. An MeOH solution (20 mL) of azpy (184 mg, 1.00 mmol) was slowly diffused to an aqueous solution (20 mL) of $Ni(ClO_4)_2\cdot 6H_2O$ (182 mg, 0.50 mmol) and NH_4SCN (152 mg, 2.00 mmol) at room temperature. After a period of a few weeks, red crystals were obtained, which were filtered out, washed with MeOH, and then dried under reduced pressure. Yield: 95 mg (0.085 mmol, 34%). Anal. Calcd for $C_{45}H_{36}N_{20}Ni_2OS_4$ (**1**·MeOH): C, 48.32; H, 3.24; N, 25.04. Found: C, 47.99; H, 3.36; N, 24.96. IR (KBr pellet) (cm^{-1}): 3468 m, 3103 w, 3078 w, 3069 w, 3045 w, 2071 s (C═N stretching), 2059 sh (C═N stretching), 1603 s, 1570 m, 1489 w, 1415 s, 1320 w, 1241 w, 1226 m, 1190 w, 1092 w, 1047 m, 1026 sh (C−O stretching), 1017 m, 846 s, 806 w, 666 w, 574 m, 550 m, 533 m, 501 w, 481 w.

Synthesis of $\{[Ni_2(NCS)_4(azpy)_4]\cdot EtOH\}_n$ (1·EtOH). The single crystals were obtained using a standard diffusion method in a straight glass tube. An EtOH solution (10 mL) of azpy (92 mg, 0.50 mmol) was slowly diffused to an aqueous solution (10 mL) of $Ni(ClO_4)_2\cdot 6H_2O$ (91 mg, 0.25 mmol) and NH_4SCN (76 mg, 1.00 mmol) at room temperature. After a period of a few weeks, red crystals were obtained, which were filtered out, washed with EtOH, and dried under reduced pressure. Yield: 26 mg (0.023 mmol, 18%). Anal. Calcd for $C_{46}H_{38}N_{20}Ni_2OS_4$ (**1**·EtOH): C, 48.78; H, 3.38; N, 24.73. Found: C, 48.11; H, 3.36; N, 24.31. IR (KBr pellet) (cm^{-1}): 3473 m, 3101 w, 3076 w, 3069 w, 3045 w, 2071 s (C═N stretching), 2057 s (C═N stretching), 1603 s, 1570 m, 1489 w, 1415 s, 1321 w, 1242 w, 1226 m, 1189 w, 1090 w, 1049 m, 1037 sh (C−O stretching), 1018 m, 847 s, 806 w, 668 w, 574 s, 551 m, 533 m, 480 w.

(3) (a) Chen, B.; Liang, C.; Yang, J.; Contreras, D. S.; Clancy, Y. L.; Lobkovsky, E. B.; Yaghi, O. M.; Dai, S. *Angew. Chem., Int. Ed.* **2006**, *45*, 1390−1393. (b) Seki, K. *Phys. Chem. Chem. Phys.* **2002**, *4*, 1968−1971. (c) Kitaura, R.; Seki, K.; Akiyama, G.; Kitagawa, S. *Angew. Chem., Int. Ed.* **2003**, *42*, 428−431. (d) Won, J.; Seo, J. S.; Kim, J. H.; Kim, H. S.; Kang, Y. S.; Kim, S.-J.; Kim, Y.; Jegal, J. *Adv. Mater.* **2005**, *17*, 80−84. (d) Kesanli, B.; Cui, Y.; Smith, M. R.; Bittner, E. W.; Bockrath, B. C.; Lin, W. *Angew. Chem., Int. Ed.* **2005**, *44*, 72−75. (e) Bu, X.-H.; Tong, M.-L.; Chang, H.-C.; Kitagawa, S.; Batten, S. R. *Angew. Chem., Int. Ed.* **2004**, *43*, 192−195. (f) Pan, L.; Adams, K. M.; Hernandez, H. E.; Wang, X.; Zheng, C.; Hattori, Y.; Kaneko, K. *J. Am. Chem. Soc.* **2003**, *125*, 3062−3067. (g) Lee, E. Y.; Jang, S. Y.; Suh, M. P. *J. Am. Chem. Soc.* **2005**, *127*, 6374−6381. (h) Takamizawa, S.; Nakata, E.; Saito, T.; Akatsuka, T. *Inorg. Chem.* **2005**, *44*, 1362−1366. (i) Kondo, M.; Shimamura, M.; Noro, S.; Minakoshi, S.; Asami, A.; Seki, K.; Kitagawa, S. *Chem. Mater.* **2000**, *12*, 1288−1299. (j) Halder, G. J.; Kepert, C. J.; Moubaraki, B.; Murray, K. S.; Cashion, J. D. *Science* **2002**, *298*, 1762−1765.

(4) (a) Kondo, M.; Yoshitomi, T.; Seki, K.; Matsuzaka, H.; Kitagawa, S. *Angew. Chem., Int. Ed. Engl.* **1997**, *36*, 1725−1727. (b) Power, K. N.; Hennigar, T. L.; Zaworotko, M. J. *New J. Chem.* **1998**, 177−181. (c) Kepert, C. J.; Rosseinsky, M. J. *Chem. Commun.* **1999**, 375−376. (d) Fletcher, A. J.; Cussen, E. J.; Prior, T. J.; Rosseinsky, M. J.; Kepert, C. J.; Thomas, K. M. *J. Am. Chem. Soc.* **2001**, *123*, 10001−10011.

(5) (a) Kitaura, R.; Kitagawa, S.; Kubota, Y.; Kobayashi, T. C.; Kindo, K.; Mita, Y.; Matsuo, A.; Kobayashi, M.; Chang, H.-C.; Ozawa, T. C.; Suzuki, M.; Sakata, M.; Takata, M. *Science* **2002**, *298*, 2358−2361. (b) Kitaura, R.; Matsuda, R.; Kubota, Y.; Kitagawa, S.; Takata, M.; Kobayashi, T. C.; Suzuki, M. *J. Phys. Chem. B* **2005**, *109*, 23378−23385. (c) Matsuda, R.; Kitaura, R.; Kitagawa, S.; Kubota, Y.; Belosludov, R. V.; Kobayashi, T. C.; Sakamoto, H.; Chiba, T.; Takata, M.; Kawazoe, Y.; Mita, Y. *Nature (London)* **2005**, *436*, 238−241. (d) Kubota, Y.; Takata, M.; Matsuda, R.; Kitaura, R.; Kitagawa, S.; Kato, K.; Sakata, M.; Kobayashi, T. C. *Angew. Chem., Int. Ed.* **2005**, *44*, 920−923. (e) Horike, S.; Matsuda, R.; Kitaura, R.; Kitagawa, S.; Iijima, T.; Endo, K.; Kubota, Y.; Takata, M. *Chem. Commun.* **2004**, 2152−2153.

(6) (a) Kondo, M.; Okubo, T.; Asami, A.; Noro, S.; Yoshitomi, T.; Kitagawa, S.; Ishii, T.; Matsuzaka, H.; Seki, K. *Angew. Chem., Int. Ed.* **1999**, *38*, 140−143. (b) Uemura, T.; Hoshino, Y.; Kitagawa, S.; Yoshida, K.; Isoda, S. *Chem. Mater.* **2006**, *18*, 992−995.

(7) Brown, E. V.; Granneman, G. R. *J. Am. Chem. Soc.* **1975**, *97*, 621−627.

Synthesis of $\{[Ni_2(NCS)_4(azpy)_4]\cdot H_2O\}_n$ ($1\cdot H_2O$). An MeOH solution (20 mL) of azpy (92 mg, 0.50 mmol) was added to an aqueous solution (20 mL) containing a mixture of $Ni(ClO_4)_2\cdot 6H_2O$ (91 mg, 0.25 mmol) and NH_4SCN (76 mg, 1.00 mmol) with a stirring in a beaker at room temperature. The orange powder obtained was collected by filtration, washed with MeOH, and dried under reduced pressure. Yield: 72 mg (0.065 mmol, 52%). Anal. Calcd for $C_{44}H_{34}N_{20}Ni_2OS_4$ ($1\cdot H_2O$): C, 47.85; H, 3.10; N, 25.36. Found: C, 47.75; H, 3.18; N, 25.18. IR (KBr pellet) (cm^{-1}): 3435 m, 3105 w, 3078 w, 3069 w, 3046 w, 2071 s (C═N stretching), 2057 sh (C═N stretching), 1603 s, 1570 m, 1488 m, 1415 s, 1321 w, 1226 m, 1190 w, 1093 w, 1049 m, 1017 m, 987 w, 967 w, 846 s, 806 w, 665 w, 573 s, 550 m, 532 m, 501 w, 481 w.

Synthesis of $\{[Ni_2(NCSe)_4(azpy)_4]\cdot MeOH\}_n$ ($2\cdot MeOH$). The single crystals were obtained using a standard diffusion method in an H-shaped cell (~50 mL). An H_2O/MeOH mixed solution (5 + 2.5 mL) containing KSeCN (72 mg, 0.500 mmol) and azpy (46 mg, 0.250 mmol) and an aqueous solution (5 mL) of $Ni(ClO_4)_2\cdot 6H_2O$ (46 mg, 0.125 mmol) were introduced into opposite sides of the H-shaped cell at room temperature. An H_2O/MeOH mixed solution (1:1) was introduced into the diffusion cell slowly. After a period of 1 month, red crystals were obtained, which were filtered out, washed with MeOH, and dried under reduced pressure. Yield: 30 mg (0.023 mmol, 37%). Anal. Calcd for $C_{45}H_{36}N_{20}Ni_2OSe_4$: C, 41.38; H, 2.78; N, 21.45. Found: C, 40.97; H, 2.80; N, 21.49. IR (KBr pellet) (cm^{-1}): 3468 m, 3099 w, 3077 w, 3067 w, 3044 w, 2074 s (C═N stretching), 2060 s (C═N stretching), 1603 s, 1569 m, 1489 w, 1415 s, 1321 w, 1226 m, 1189 w, 1048 m, 1025 sh (C−O stretching), 1018 m, 985 w, 846 s, 667 w, 573 m, 551 m, 533 w, 501 w, 435 w.

Synthesis of $\{[Ni_2(NCSe)_4(azpy)_4]\cdot H_2O\}_n$ ($2\cdot H_2O$). An aqueous solution (10 mL) of KSeCN (144 mg, 1.00 mmol) was added to an MeOH solution (10 mL) of azpy (92 mg, 0.500 mmol) at room temperature. An aqueous solution (10 mL) of $Ni(ClO_4)_2\cdot 6H_2O$ (91 mg, 0.250 mmol) was added to the resulting red solution with a stirring in a beaker. The orange powder obtained was collected by filtration, washed with H_2O and MeOH, and dried under reduced pressure. Yield: 136 mg (0.11 mmol, 84%). Anal. Calcd for $C_{44}H_{34}N_{20}Ni_2OSe_4$ ($2\cdot H_2O$): C, 40.90; H, 2.65; N, 21.68. Found: C, 41.08; H, 2.65; N, 21.68. IR (KBr pellet) (cm^{-1}): 3467 m, 3101 w, 3077 w, 3069 w, 3046 w, 2074 s (C═N stretching), 2057 sh (C═N stretching), 1603 s, 1569 m, 1489 w, 1415 s, 1321 w, 1226 m, 1191 w, 1094 w, 1049 m, 1018 m, 846 s, 665 w, 573 m, 551 w, 533 w, 500 w, 436 w.

Physical Techniques. Elemental analysis (for C, H, and N) was performed using a Perkin-Elmer model 240C elemental analyzer. The IR spectra (400−4000 cm^{-1}) were recorded on a Perkin-Elmer Spectrum 2000 spectrometer with the samples prepared as KBr pellets. A high-temperature transmission cell, HT-32 (Thermo Spectra-Tech), was used to measure the temperature dependence of the IR spectra. The Raman spectra were recorded on powdered and crystalline samples using a JASCO RMP-210 portable laser Raman spectrophotometer equipped with a 100 mW LD-pumped Nd:YAG laser emitting at 532 nm. The XRD data were collected using a Rigaku RINT-UltimaIII diffractometer employing Cu Kα radiation. Thermogravimetric analysis (TGA) was performed using a Rigaku Thermo Plus 2/TG-DTA8120 over the temperature range 25−500 °C in an N_2 atmosphere.

Gas Adsorption Measurements. The N_2 sorption isotherms at −196 °C were measured using a Belsorp18 volumetric adsorption apparatus (Bel Japan, Inc.). The sorption isotherms for N_2 and CH_4 at 25 °C were performed using a model FMS-BG automatic gravimetric adsorption apparatus (Bel Japan, Inc.). Prior to the adsorption measurements being carried out, a known weight of the as-synthesized sample was dried under high vacuum at 80 °C for a period of several hours to remove the guest molecules. The saturated amount of adsorption, W_L, was determined from the Langmuir plot. The high-pressure adsorption of supercritical gas in micropores has been characterized using the extended Dubinin−Radushkevich (DR) equation.[8] From the DR equation, we obtain the parameter βE_0 (in units of kJ·mol^{-1}), where E_0 and β are the characteristic adsorption energy and the affinity coefficient, and the quasi-saturated vapor pressure P_{0q} (in atm). The value of βE_0 is associated with the isosteric heat of adsorption, $q_{st,\phi = 1/e}$, at the fractional filling of $\phi = 1/e$ using the enthalpy of vaporization, ΔH_v, at the boiling point.

Crystal Structure Determination. Suitable crystals of $1\cdot$MeOH, $1\cdot$EtOH, **1**, $2\cdot$MeOH, and **2** were mounted on a glass fiber. All the measurements were performed using a Rigaku RAXIS-RAPID imaging plate diffractometer with graphite-monochromated Mo Kα radiation ($\lambda = 0.710\ 69$ Å). An empirical absorption correction was applied to the data,[9] and the data were corrected for Lorentz and polarization effects. The structure of $1\cdot$MeOH was resolved using direct methods (SHELXS-97)[10] and expanded using Fourier techniques.[11] The structures of the other compounds were resolved using the final atomic coordinates of isomorphous $1\cdot$MeOH as the initial coordinates, and these were expanded using Fourier techniques.[11] The non-hydrogen atoms were refined anisotropically. All the hydrogen atoms were refined using the riding model. The refinements were carried out using a full-matrix least squares technique on F^2. All the calculations were performed using the CrystalStructure crystallographic software package.[12] The crystal data and details of the structure determinations are summarized in Table 1.

Crystallographic data for the structures reported in this paper have been deposited at the Cambridge Data Centre as Supplementary Publication Nos. CCDC-603570 ($1\cdot$MeOH), -603569 ($1\cdot$EtOH), -603568 (**1**), -603572 ($2\cdot$MeOH), and -603571 (**2**). Copies of the data can be obtained free of charge on application to CCDC, 12 Union Road, Cambridge CB2 1EZ, U.K. (Fax: (+44) 1223-336-033. E-mail: deposit@ccdc.cam.ac.uk.)

Results and Discussion

The compounds $1\cdot$MeOH, $1\cdot$EtOH, **1**, $2\cdot$MeOH, and **2** form isomorphous coordination frameworks. Figure 1a shows an ORTEP view around the Ni^{II} center of $1\cdot$MeOH. There are two crystallographically independent Ni^{II} centers in the $1\cdot$MeOH crystal. The Ni(1) center has a slightly shortened octahedral geometry with four pyridine nitrogen atoms (Ni−N = 2.112(3) and 2.108(4) Å) and two trans isothiocyanate nitrogen atoms (Ni−N = 2.073(4) Å), while the Ni(2) center has a definite shortened octahedral environment with the same ligands as the Ni(1) center (Ni−N(py) = 2.118(3) and 2.128(4) Å; Ni−N(NCS) = 2.033(3) Å). The

(8) (a) Kaneko, K. *Langmuir* **1987**, *3*, 357−363. (b) Kaneko, K.; Murata, K.; Shimizu, K.; Camara, S.; Suzuki, T. *Langmuir* **1993**, *9*, 1165−1167. (c) Kaneko, K.; Murata, K. *Adsorption* **1997**, *3*, 197−208.
(9) Abscor: Higashi, T. *Empirical Absorption Correction based on Fourier Series Approximation*; Rigaku Corp.: Tokyo, Japan, 1995.
(10) SHELXS-97: Sheldrick, G. M. *Acta Crystallogr.* **1990**, *A64*, 467−473.
(11) DIRDIF-94: Beurskens, P. T.; Admiraal, G.; Beurskens, G.; Bosman, W. P.; de Gelder, R.; Israel, R.; Smits, J. M. M. *The DIRDIF-94 program system*; Technical Report of the Crystallography Laboratory, University of Nijmegen: Nijmegen, The Netherlands, 1994.
(12) CrystalStructure 3.7.0: *Crystal Structure Analysis Package*; Rigaku and Rigaku/MSC: The Woodlands, TX, 2000−2005.

Table 1. Crystallographic Data

(a) Data for $\{[Ni_2(NCS)_4(azpy)_4]\cdot MeOH\}_n$ (**1**·MeOH), $\{[Ni_2(NCS)_4(azpy)_4]\cdot EtOH\}_n$ (**1**·EtOH), and $[Ni_2(NCS)_4(azpy)_4]_n$ (**1**)

param	**1**·MeOH	**1**·EtOH	**1**
formula	$C_{45}H_{36}N_{20}Ni_2OS_4$	$C_{46}H_{38}N_{20}Ni_2OS_4$	$C_{44}H_{32}N_{20}Ni_2S_4$
fw	1118.55	1132.58	1086.51
lattice	orthorhombic	orthorhombic	orthorhombic
a, Å	18.003(2)	17.952(2)	17.9172(17)
b, Å	30.929(4)	30.817(4)	31.246(3)
c, Å	19.443(3)	19.435(4)	19.332(2)
V, Å^3	10827(3)	10752(3)	10822.9(20)
space group	*Ccca* (No. 68)	*Ccca* (No. 68)	*Ccca* (No. 68)
Z	8	8	8
ρ(calcd), g cm^{-3}	1.372	1.399	1.334
F(000)	4592.00	4656.00	4448.00
μ(Mo Kα), cm^{-1}	9.04	9.11	9.01
temp, °C	−50	−100	0
R^a	0.038 ($I > 3.00\sigma(I)$)	0.045 ($I > 2.00\sigma(I)$)	0.041 ($I > 2.00\sigma(I)$)
$R_w{}^b$	0.073 ($I > 3.00\sigma(I)$)	0.068 ($I > 2.00\sigma(I)$)	0.057 ($I > 2.00\sigma(I)$)
no. of observns	2421	2566	3829
no. of variables	352	351	333

(b) Data for $\{[Ni_2(NCSe)_4(azpy)_4]\cdot MeOH\}_n$ (**2**·MeOH) and $[Ni_2(NCSe)_4(azpy)_4]_n$ (**2**)

param	**2**·MeOH	**2**
formula	$C_{45}H_{36}N_{20}Ni_2OSe_4$	$C_{44}H_{32}N_{20}Ni_2Se_4$
fw	1306.15	1274.11
lattice	orthorhombic	orthorhombic
a, Å	18.092(3)	18.154(2)
b, Å	31.514(5)	31.786(3)
c, Å	19.150(2)	19.053(2)
V, Å^3	10918(3)	10994(2)
space group	*Ccca* (No. 68)	*Ccca* (No. 68)
Z	8	8
ρ(calcd), g cm^{-3}	1.589	1.539
F(000)	5168.00	5024.00
μ(Mo Kα), cm^{-1}	34.11	33.84
Temp, °C	−180	0
R^a	0.056 ($I > 3.00\sigma(I)$)	0.038 ($I > 2.00\sigma(I)$)
$R_w{}^b$	0.065 ($I > 3.00\sigma(I)$)	0.051 ($I > 2.00\sigma(I)$)
no. of observns	4616	3718
no. of variables	352	333

[a] $R = \sum||F_o| - |F_c||/\sum|F_o|$. [b] $R_w = [\sum w(|F_o| - |F_c|)^2/\sum wF_o^2]^{1/2}$.

Ni−N−C bonds of the NCS^- ligands are distorted from 180°; the Ni(1)−N(9)−C(21) bond angle (148.9(4)°) is considerably more distorted than the Ni(2)−N(10)−C(22) bond angle (160.4(3)°), due to the different environment around the S atom (vide infra). The N−C−S bond angles are almost linear (178.4(4) and 178.9(4)°).

The azpy ligands bridge the Ni^{II} centers to form 2-D layers with large rhombus grids (dimensions = ca. 9 × 8 Å^2) with corner angles of ca. 86 and 94°, as illustrated in Figure 1b. These sheets have approximately perpendicular interpenetration, giving rise to a tight 3-D structure, as shown in Figure 1c. Despite this interpenetration, the network forms small 1-D channels (ultramicropores) running parallel with the *c*-axis. Half of these channels are occupied by MeOH molecules, generating a checkerboard-type pattern. This alternating distribution causes the framework to distort away from regular interpenetration so that the occupied and empty channels have windows with dimensions of ca. 1.2 × 2.7 and 1.2 × 1.6 Å^2 and relative crystal volumes of 8.8% and 2.6%, respectively.[13,14] In the 1-D channels, the MeOH guest molecules are well separated from each other with a period of ca. 9.5 Å along the *c*-axis. Such a periodicity and a small window size indicate that **1**·MeOH does not have straight channels but has periodic channels instead. Similar interpenetrated networks with azpy ligands have been reported in $\{[M_2(NCS)_4(azpy)_4]\cdot EtOH\}_n$ (M = Co and Fe).[3i,j]

The MeOH guest molecules interact with the host frameworks through a characteristic hydrogen-bonding interaction of −S···HO− bonds. Inorganic counteranions, such as NO_3^-, SO_4^{2-}, BF_4^-, PF_6^-, ClO_4^-, and NCS^-, can be contained within coordination polymers with metal cations and neutral bipyridine-type ligands. These play an important role in the assembly of framework motifs, the stability of porous frameworks, and the uptake of guest molecules through hydrogen-bonding interactions. In particular, the introduction of hydrogen-bonding sites by inorganic counteranions is one of the available methods for modifying the pore walls of microporous coordination polymers. We focused on the NCS^- and $NCSe^-$ anions, as these anions have a strong coordination ability and, therefore, are used as terminal or bridging ligands in microporous coordination polymers.[3j,15] Although S is normally a weaker hydrogen bond acceptor than O is, it can be regarded as a conventional hydrogen

(13) The size was measured by considering van der Waals radii for the constituent atoms.

(14) Spek, A. L. *PLATON, A Multipurpose Crystallographic Tool*; Utrecht University: Utrecht, The Netherlands, 2003.

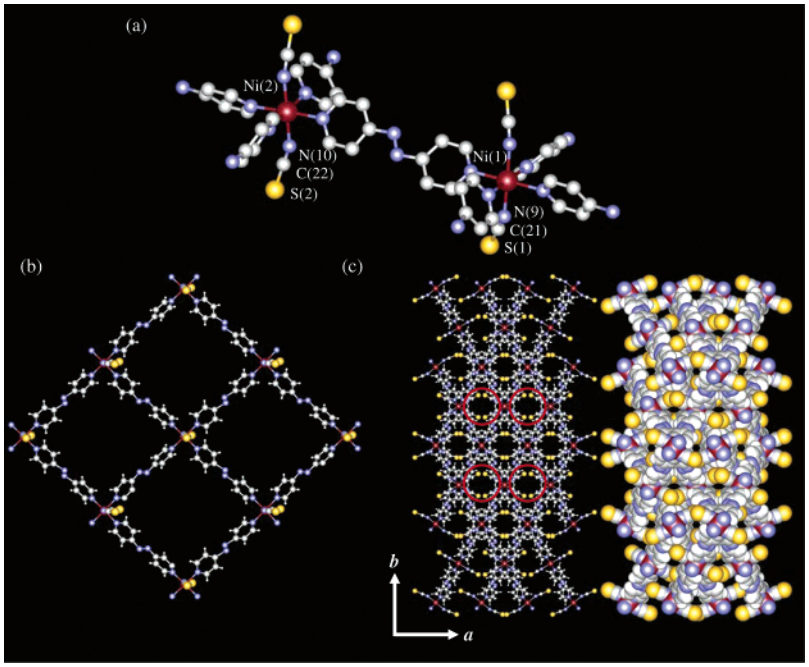

Figure 1. Structure of **1**·MeOH: (a) view of the Ni^{II} centers (hydrogen atoms have been omitted for clarity); (b) view of the 2-D layer; (c) view of the porous framework represented by a ball-and-stick model (left) and a CPK model (right). The guest MeOH molecules, which are included in the channels denoted by the red circles, have been omitted for clarity. The vermilion, blue, yellow, gray, and white colors represent nickel, nitrogen, sulfur, carbon, and hydrogen atoms, respectively.

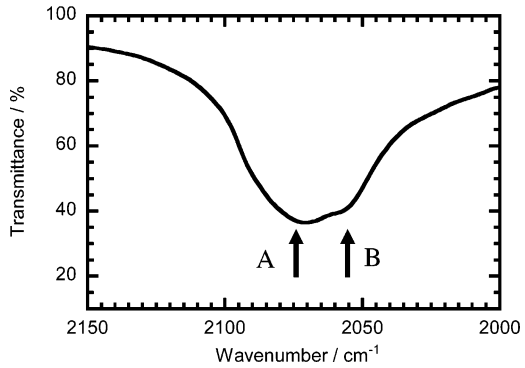

Figure 2. IR spectra of **1**·MeOH in the C═N stretching region.

bond acceptor.[16] Nevertheless, this acceptor has been neglected in classical overviews of hydrogen bonding. In **1**·MeOH, the S···O bond length is 3.51(2) Å, whose value is comparable with that in $\{[Fe_2(NCS)_4(azpy)_4]\cdot EtOH\}_n$ (3.453(10) and 3.83(2) Å).[3j] Interestingly, the MeOH guest molecule is captured only by the S(1) atom, while the S(2) atom is free to form hydrogen bonds with the MeOH. This difference in the hydrogen-bonding interaction around the S atoms was also confirmed by the IR and Raman spectra. In perfect trans symmetry at Ni^{II} centers, the mutual exclusion principle demands that the asymmetric stretch is infrared active, and the symmetric stretch is observable only in the Raman spectra.[17] The IR (Figure 2) and Raman (Figure S3, Supporting Information) spectra of **1**·MeOH show two types of C═N stretching vibration modes (A and B). Furthermore, the temperature dependence of the IR spectra of **1**·MeOH (Figure S4) indicates that peak A is derived from the hydrogen-bonded NCS^- anions and peak B is derived from the free-state hydrogen bonds.

To investigate the crystal structure after the removal of the MeOH molecules, X-ray diffraction was used to analyze desolvated crystals of **1** obtained by heating a single crystal of **1**·MeOH at 150 °C under reduced pressure. No residual electron density was observed in the channels, which is consistent with the complete desorption of MeOH. However, the coordination framework was almost unchanged, which is in sharp contrast to $\{[Fe_2(NCS)_4(azpy)_4]\cdot EtOH\}_n$,[3j] which undergoes a recognizable structural change. After the removal of the guest MeOH molecules, the Ni(1)−N(9)−C(21) bond angle (149.3(2)°) was still more deformed than the Ni(2)−N(10)−C(22) bond angle (162.3(2)°). This structural difference is well reflected in the position of the C═N stretching vibration in the guest-free state (Figure S4).

We synthesized isostructural Ni^{II} coordination polymers with other guest molecules, $\{[Ni_2(NCS)_4(azpy)_4]\cdot EtOH\}_n$ (**1**·EtOH) and $\{[Ni_2(NCS)_4(azpy)_4]\cdot H_2O\}_n$ (**1**·H_2O). The X-ray diffraction analysis of **1**·EtOH showed similar −S···HO− hydrogen bonds between the isothiocyanate ligands and the EtOH molecules (S···O = 3.452(14) Å). Although single crystals of **1**·H_2O could not be obtained, the XRD pattern of the powder sample of **1**·H_2O is similar to that calculated from the result of the single-crystal X-ray diffraction measurements of **1**·MeOH (Figure S18), indicating the formation of an isostructural framework.[18] The IR and Raman

(15) (a) Sekiya, R.; Nishikiori, S.; Ogura, K. *J. Am. Chem. Soc.* **2004**, *126*, 16587−16600. (b) Uemura, K.; Kitagawa, S.; Kondo, M.; Fukui, K.; Kitaura, R.; Chang, H.-C.; Mizutani, T. *Chem.—Eur. J.* **2002**, *8*, 3587−3600.

(16) Desiraju, G. R.; Seteiner, T. *The Weak Hydrogen Bond*; Oxford University Press: New York, 1999.

(17) Herber, R. H.; Nan, G. *Inorg. Chem.* **1988**, *27*, 2644−2647.

(18) We calculated the cell parameters of **1**·H_2O using the UnitCell software:[19] a = 18.08(2), b = 31.19(5), c = 19.43(4) Å; V = 10960(21) $Å^3$.

Table 2. Volume and Minimum Dimensions of the Guests Molecules Used in This Work

guest	V (Å^3)	min dimens (Å^2)
H_2O	27.7	2.92 × 3.23
N_2	35.6	2.99 × 3.05
CH_4	43.4	3.83 × 3.94
MeOH	53.4	3.81 × 4.18
EtOH	75.8	4.16 × 4.27

spectra of **1**·H_2O indicate the formation of hydrogen-bonding interactions between the NCS^- anions and the H_2O guest molecules as well as **1**·MeOH and **1**·EtOH. The TGA result of **1**·H_2O also supports the presence of the H_2O guest molecules (see the Supporting Information).

Table 2 lists the volume and dimensions of the guest molecules used in this work.[20,21] The porous framework **1** has a guest-accessible volume of 1234 Å^3/unit cell, i.e., ∼150 Å^3/cavity. This value is large enough to accommodate the guest molecules listed in Table 2. The isostructural coordination polymer $[Fe_2(NCS)_4(azpy)_4]_n$ can even incorporate 1-PrOH guest molecules.[3j,22]

Interestingly, the molecular dimensions of the MeOH guest molecule are noticeably larger than the size of the channel window (ca. 1.2 × 2.7 Å^2). Therefore, the passage of the guest molecule through the windows requires an expansion of the unit cell, which would be clearly manifested in a change of the lattice parameters, but the X-ray diffraction data collected from the MeOH-loaded and desolvated materials showed no change in crystal structure in response to the ingress and loss of MeOH. The passage of MeOH through the windows must therefore proceed by an expansion of the window size for only as long as is required for the passage of an MeOH molecule. The structure then relaxes back to the original structure. It is important to recall that the porous framework is thermally stable to 200 °C, demonstrating that

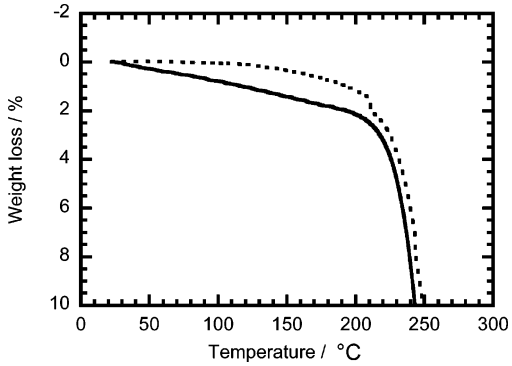

Figure 3. Thermogravimetric curves of **1**·MeOH (solid line) and **1**·EtOH (dashed line).

the oversized guest molecules are dynamically distorting a structure that is not intrinsically unstable. The reason for such a dynamics is probably that the channels are created by assembling the 2-D motifs via an interpenetration that is not a chemically bonded network but is merely a mechanical entanglement. Similar unique framework dynamics have been reported for another porous coordination polymer, $[Ni_2(4,4'\text{-bpy})_3(NO_3)_4]_n$,[4c,d] in which 1-D ladder motifs are assembled by C−H···O hydrogen bonding between the oxygen atoms of the nitrate groups and the 4,4′-bpy molecules at a distance of 2.72(2) Å.

TGA was used to investigate the desorption behavior of the guest molecules. The TGA curves of **1**·MeOH and **1**·EtOH showed no clear step corresponding to guest desorption, as illustrated in Figure 3. The MeOH guest molecules were released gradually from the channels. The EtOH guest molecules were retained stably in the channels up to a temperature of 80 °C, and these were then ejected more slowly than the MeOH guest molecules. Such a marked difference is possibly due to the difference in van der Waals interactions in the ultramicropores and/or an entrance blocking effect at the pore windows. An increase in the alkyl chain length would enhance the van der Waals interaction with the pore walls.[3a] On the other hand, as the pore window size is similar to the minimum dimensions of the guest molecule, an entrance blocking effect would influence the adsorption behavior.[23] The observed shape and/or size dependency on the desorption behavior is a characteristic feature of porous materials containing channels whose size is comparable of that of the guest molecules.

Next, we used an isoselenocyanate ligand $NCSe^-$ instead of NCS^- to modify the porous functionalities, forming $\{[Ni_2(NCSe)_4(azpy)_4]\cdot MeOH\}_n$ (**2**·MeOH) and $\{[Ni_2(NCSe)_4(azpy)_4]\cdot H_2O\}_n$ (**2**·H_2O). Se has a larger van der Waals radius of 1.90 Å compared to S (1.80 Å). The crystal structure of **2**·MeOH is also isostructural with **1**·MeOH. The occupied and empty channels of **2**·MeOH have windows with dimensions of ca. 0.8 × 3.2 and 0.8 × 1.6 Å^2 and relative crystal volumes of 8.3% and 2.8%, respectively,[13,14] similar to **1**·MeOH. Although Se has an electronegativity similar to that of S (2.4 and 2.5, respectively), examples that show hydrogen-bonding interactions via Se are scant.[16] In **2**·

(19) UnitCell: Holland, T. J. B.; Redfern, S. A. T. Unit cell refinement from powder diffraction data: the use of regression diagnostics. *Mineral. Mag.* **1997**, *61*, 65−77.

(20) The molecular volume was calculated using the Gaussian03W software package, employing B3LYP/6-311G* basis sets and the keyword "volume".

(21) (a) Fletcher, A. J.; Cussen, E. J.; Prior, T. J.; Rosseinsky, M. J.; Kepert, C. J.; Thomas, K. M. *J. Am. Chem. Soc.* **2001**, *123*, 10001−10011. (b) Webster, C. E.; Drago, R. S.; Zerner, M. C. *J. Am. Chem. Soc.* **1998**, *120*, 5509−5516.

(22) We checked the shape-selective uptake for 1-PrOH and 2-PrOH in **1**. The molecular volumes of both guest molecules (99.3 and 99.5 Å^3 for 1-PrOH and 2-PrOH, respectively)[20] are smaller than the cavity volume (∼150 Å). When the desolvated sample **1** is immersed in 1-PrOH or 2-PrOH solution, both alcohols are inserted into the ultramicropores. Although no clear C−O stretching vibration was observed in the IR spectra, the thermogravimetric curves show the presence of 1-PrOH and 2-PrOH guest molecules in the ultramicropores (see the Supporting Information). The XRD patterns of the guest-exchanged samples, **1**·*x*(1-PrOH) and **1**·*x*(2-PrOH), are similar to that calculated from the result of the single-crystal X-ray diffraction measurements of **1**·MeOH (Figure S20), indicating the retention of the original framework. We calculated the cell parameters of **1**·*x*(1-PrOH) and **1**·*x*(2-PrOH) using the UnitCell software: a = 18.36(4) Å, b = 31.38(8) Å, c = 19.35(7) Å, and V = 11150(33) Å^3 for **1**·*x*(1-PrOH); a = 18.27(3) Å, b = 31.39(7) Å, c = 19.39(6) Å, and V = 11120(29) Å^3 for **1**·*x*(2-PrOH). The cell volumes of **1**·*x*(1-PrOH) and **1**·*x*(2-PrOH) are larger than that of **1**·H_2O, which may be attributed to the difference in the guest volumes incorporating into ultramicropores. The observed nonselective uptake indicates that the shape of the cavity in **1** permits the insertion of both 1- and 2-PrOH guest molecules.

(23) Li, D.; Kaneko, K. *J. Phys. Chem. B* **2000**, *104*, 8940−8945.

MeOH, characteristic −Se···HO− hydrogen bonds occur between the isoselenocyanate ligands and the MeOH molecules (Se···O = 3.64(2) Å). The IR and Raman spectra (see the Supporting Information) indicate the presence of both hydrogen-bonding and nonbonding $NCSe^-$ anions, as well as **1**·MeOH. Although single crystals of **2**·H_2O could not be obtained, the XRD pattern of the powder sample of **2**·H_2O is similar to that calculated from the result of the single-crystal X-ray diffraction measurements of **2**·MeOH (Figure S19), indicating the formation of isostructural framework.[24] The IR and Raman spectra of **2**·H_2O indicate the formation of hydrogen bonding interactions between the $NCSe^-$ anions and the H_2O guest molecules as well as **2**·MeOH. The TGA result of **2**·H_2O also supports the presence of the H_2O guest molecules (see the Supporting Information). Although the desorption behaviors of **2**·MeOH and **2**·H_2O were compared with those of **1**·MeOH and **1**·H_2O using TGA (see the Supporting Information), no sharp contrast was observed. These results indicate that the porous properties (shape, size, volume, and desorption behavior) are less affected by the replacement of S by Se. As well as **1**·MeOH, the desolvated crystal **2** obtained by heating a single crystal of **2**·MeOH at 170 °C under reduced pressure retained its original framework, which was checked using X-ray diffraction analysis.

From the results of the X-ray diffraction analysis, it was revealed that the porous framework of **1** is retained after removal of the guest molecules. Compound **1** can incorporate a variety of guest molecules with a hydroxy substituent via hydrogen bonds. We then investigated the adsorption properties of other guest molecules, N_2 and CH_4, in **1**. To obtain **1** without any guest molecules, a known weight of **1**·H_2O was dried under high vacuum at 80 °C for a period of several hours. The adsorption isotherm of N_2 with **1** measured at −196 °C is shown in Figure 4a. The isotherm shows a gradual increase in all regions, which is associated with the strong entrance blocking effect.[23] The molecular dimensions of N_2 (listed in Table 2) are larger than the pore window size of **1**. In addition, the low-temperature prevents any framework distortion. Therefore, it is difficult for N_2 to diffuse through the small pore windows into the inside of the channels at low temperatures. The small BET surface area of 22 $m^2 \cdot g^{-1}$ also indicates the adsorption occurred at the surface and not in the channels. On the other hand, the adsorption isotherms of N_2 and CH_4 measured at high pressure and at 25 °C showed a type I curve according to the IUPAC classification, as shown in Figure 4b. Because N_2 and CH_4 are supercritical gases near to room temperature, they are not adsorbed on the surface but into the microporous channels. The entrance blocking effect weakens with increasing temperature, which permits the N_2 and CH_4 gas to diffuse deeply into the channels. Table 3 summarizes the micropore parameters of **1**. The value of $q_{st,\phi=1/e}$ = 14.4 $kJ \cdot mol^{-1}$ for N_2 gas is comparable to that of pitch-based activated carbon fiber (pore width = 7.5−14.5 Å) at 30 °C ($q_{st,\phi=1/e}$ = 13.8−14.4 $kJ \cdot mol^{-1}$).[10c] On the other hand, the value of $q_{st,\phi=1/e}$ = 20.4 $kJ \cdot mol^{-1}$ for CH_4 is considerably larger than those of Cu-4,4′-bpy and Cu−dicarboxylate porous coordination polymers (pore width = 7−11 Å, $q_{st,\phi=1/e}$ = 16−17 $kJ \cdot mol^{-1}$),[25] and activated carbon fibers and superhigh surface area carbons (pore width = 8−16 Å, $q_{st,\phi=1/e} \sim 17$ $kJ \cdot mol^{-1}$),[10b,c] which clearly indicates that **1** containing ultramicropores has deeper potential wells for CH_4 than the other porous materials do.[26]

As shown in Table 2, the N_2 and CH_4 guest molecules used in our adsorption measurements have considerably larger molecular dimensions, 2.99 × 3.05 and 3.83 × 3.94 $Å^2$, respectively, than the window size of the ultramicropores (1.2 × 2.7 $Å^2$). Nevertheless, such gases are incorporated deeply into the ultramicropores at room temperature without inducing a framework collapse. These results indicate that the guest molecules without any special substituents also

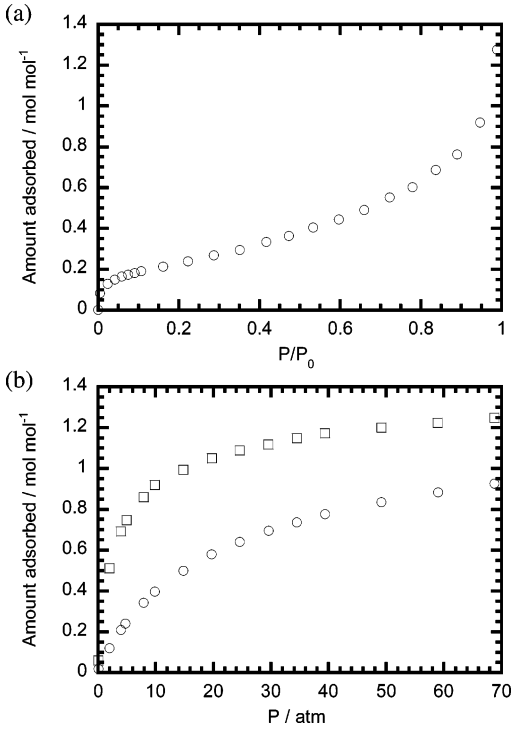

Figure 4. (a) Adsorption isotherm of nitrogen with **1** at −196 °C in the relative pressure range from 10^{-3} to 0.99. P_0 denotes the saturated vapor pressure, 101 kPa of nitrogen at −196 °C. (b) Adsorption isotherms of nitrogen (open circles) and methane (open squares) with **1** at 25 °C in the pressure range 0.09−68.8 atm.

Table 3. Micropore Parameters of **1** Obtained from the Langmuir and DR Analysis

adsorbate	W_L ($mmol \cdot g^{-1}$)	P_{0q} (atm)	βE_0 ($kJ \cdot mol^{-1}$)	$q_{st,\phi=1/e}$ ($kJ \cdot mol^{-1}$)
N_2	1.15	463	8.85	14.4
CH_4	1.19	185	12.2	20.4

(24) We calculated the cell parameters of **2**·H_2O using the UnitCell software:[19] a = 18.32(3), b = 31.65(4), c = 19.17(3) Å; V = 11120(19) $Å^3$.

(25) (a) Noro, S.; Kitaura, R.; Kondo, M.; Kitagawa, S.; Ishii, T.; Matsuzaka, H.; Yamashita, M. *J. Am. Chem. Soc.* **2002**, *124*, 2568−2583. (b) Noro, S.; Kitagawa, S.; Kondo, M.; Seki, K. *Angew. Chem., Int. Ed.* **2000**, *39*, 2082−2084. (c) Seki, K.; Mori, W. *J. Phys. Chem. B* **2002**, *106*, 1380−1385.

(26) In the ultramicropores, CH_4 molecules can interact with the aromatic pyridine rings at the pore walls via CH−π interactions.[27]

(27) (a) Takamizawa, S.; Nakata, E.; Saito, T.; Akatsuka, T. *Inorg. Chem.* **2005**, *44*, 1362−1366. (b) Sozzani, P.; Bracco, S.; Comotti, A.; Ferretti, L.; Simonutti, R. *Angew. Chem., Int. Ed.* **2005**, *44*, 1816−1820.

induce an expansion of the window size for only as long as is required for the passage of the N_2 and CH_4 molecules.

Conclusions

Novel Ni^{II}−NCS(Se)−azpy coordination polymers, $\{[Ni_2(NCX)_4(azpy)_4]\cdot G\}_n$ (X = S, G = MeOH (**1**·MeOH); X = S, G = EtOH (**1**·EtOH); X = S, G = H_2O (**1**·H_2O); X = S, G = no guest (**1**); X = Se, G = MeOH (**2**·MeOH); X = Se, G = H_2O (**2**·H_2O); X = Se, G = no guest (**2**)), with characteristic ultramicropores have been structurally characterized using X-ray diffraction measurements. Their framework stability and porous functionality have also been investigated. The ultramicroporous framework, which has small pore windows with dimensions of ca. 1.2 × 2.7 and 1.2 × 1.6 Å^2 for **1**·MeOH and ca. 0.8 × 3.2 and 0.8 × 1.6 Å^2 for **2**·MeOH, is constructed by the interpenetration of 2-D $[Ni(NCX)_2(azpy)_2]_n$ (X = S or Se) layers. The NCS^- and $NCSe^-$ anions are exposed to the channel walls and interact with guest molecules having −OH groups, such as H_2O, MeOH, and EtOH, via −S(Se)···OH− hydrogen bonds. The structures of the desolvated compounds **1** and **2** are almost same as those of **1**·MeOH and **2**·MeOH, indicating that the ultramicropores are stable without any guest molecules. The adsorption and desorption experiments indicate that **1** and **2** have dynamic 1-D ultramicroporous channels constructed by an interpenetration that is not a chemical bonding network but merely a mechanical entanglement. Work is now in progress to investigate the adsorption selectivity of these compounds using a variety of guest molecules.

Acknowledgment. This work was partly supported by a Grant-in-Aid for Scientific Research on Priority Areas (No. 434 "Chemistry of Coordination Space") from the Ministry of Education, Science, Sports, and Culture of Japan.

Supporting Information Available: X-ray crystallographic data for **1**·MeOH, **1**·EtOH, **1**, **2**·MeOH, and **2**, in CIF format, the MeOH guest molecule array in **1**·MeOH, a view of the hydrogen-bonding interactions between the host networks and the MeOH guest molecules in **1**·MeOH, Raman spectra of **1**·MeOH, temperature dependence of the IR spectra of **1**·MeOH, time dependence of the IR spectra of **1**·MeOH at 150 °C, IR and Raman spectra of **1**·H_2O, **1**·EtOH, **2**·H_2O, and **2**·MeOH, EtOH guest molecule array in **1**·EtOH, thermogravimetric curves of **1**·H_2O, **1**·*x*(1-PrOH), **1**·*x*(2-PrOH), **2**·H_2O, and **2**·MeOH, IR spectra of **1**·*x*(1-PrOH) and **1**·*x*(2-PrOH), and XRD patterns of **1**·H_2O, **2**·H_2O, **1**·*x*(1-PrOH), and **1**·*x*(2-PrOH). This material is available free of charge via the Internet at http://pubs.acs.org.

IC061052D